Data Fusion of Airborne Hyperspectral and Full Waveform LiDAR Data for Land Cover Classification

Kuei-Chia Chen [1], Chun-Yu Liu[1], Chi-Kuei Wang[1*], Hone-Jay Chu[1], Guo-Hao Huang[1]
[1]National Cheng Kung University, No. 1, University Road, Tainan City 701, Taiwan

*Corresponding author: chikuei@mail.ncku.edu.tw

ABSTRACT

Land use classification is vital in understanding ecosystems and evaluating nature sources. Substantial studies have been done on employing the reflectance spectra from hyperspectral images to classify land cover. It is known that the full waveform LiDAR system can obtain the high-precision 3D elevation information, and the shape of the waveform packet describes the characteristics of the surface. In this study, we present an efficient approach that integrates hyperspectral images and full waveform Lidar data for detecting land use clusters.

Our study area is located in upper stream of Tsengwen Reservoir watershed in Taiwan. The 72-band hyperspectral data were obtained by an Itres CASI-1500 with a pixel resolution of 1 m. The spectrum range of Itres CASI-1500 is between 362.8 and 1051.3 nm, and the spectral resolution is 9.6 nm. The Lidar data were acquired by an ALTM Pegasus with a point density of 2 points/m^2.

We employed Minimum Noise Component (MNF) and Principal Components Analysis (PCA) for data fusion of multivariate statistical models. Based on fused data, Maximum Likelihood was applied to image classification. The classification results showed that fusing the full waveform LiDAR data and the hyperspecrtal data can slightly increase the classification accuracy.

Keywords: Full waveform lidar systems, Hyperspectral imagery, Image fusion, Principal component analysis, Minimum noise fraction

INTRODUCTION

Remote sensing techniques have extensively used to describe the land cover for resources survey and environmental monitoring. Most of the remote sensing data can obtain the surface of spectral reflectance data. Hyperspectral image was improved the classification accuracy of land covers with similar spectral characteristical, such as the complex landscapes (Borengasser et al., 2008). Narrow-band spectral images can provide more detailed information among hyperspectral sensor. These precious data sources are the surface reflectance of passive sensor information.

LiDAR system is an active sensor and has been employed in many detection techniques. LiDAR system not only can get the digital elevation model (DEM) and the digital surface model at the same time. The waveform LiDAR system record the laser beam intensity of returned signal over time. So, the application of lidar data to study of forest environmental or land type include the tree crowns are delineated from the canopy height model (CHM), forest gap dynamics, and landcover classification (Joshua et al., 2009; Udayalakshmi et al., 2008; Reitberger et al, 2008; Giovann et al., 2012).

These data of above can be used for land cover classification. In order to understand the vertical information contributions in the land cover classification. In this paper, we tested the full waveform lidar system, to attempt the fusion of hyperspectral image and full waveform LiDAR data for the different land cover classification. Pohl and Genderen (1998) suggested that the fusion level would be at pixel level. As a result, the new image is composed of each source image.

MATERIALS AND METHODS / EXPERIMENTAL

The study was conducted on a 35 km2 area, which are located at the upstream of Tseng-Wen River in South-Taiwan (LU：214127.268, 2582880.695; RD：219127.268, 2575880.695), (Figure 1). The left half of the study area are mostly uncultivated areas, others are cultivation of agricultural industrial crop areas. The land cover type included that water river (WR), mixed forest (MF),

grasslands (GL), tea farm (TF), areca farm (AF), bare soil (BS), and urban fabric (UF). Hence, the 7 land cover classes are used for classification.

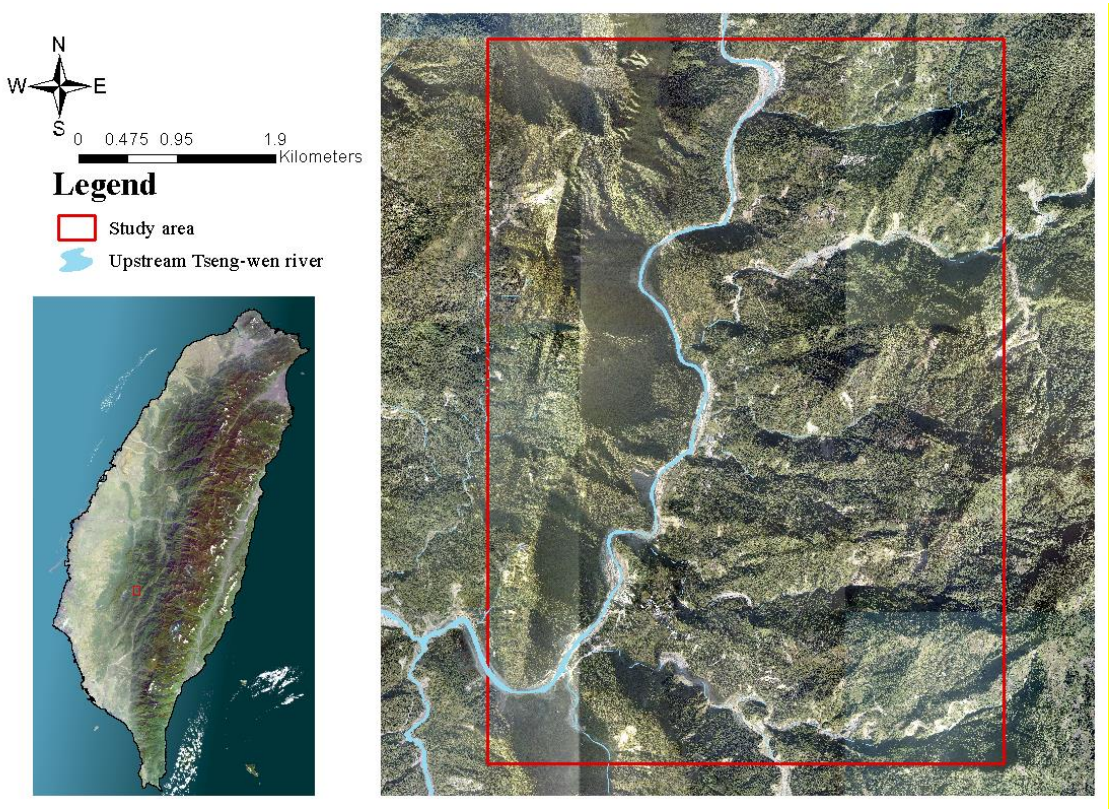

Figure 1. Study area: the upstream Tseng-Wen River in South-Taiwan. The land cover type included that water river, mixed forest, grasslands, tea farm, areca farm, bare soild, and urban fabric.

In this study, Optech ALTM Pegasus with medium format camera (Dimac Ultralight + 60MP) and Itres CASI-1500 were used to acquire the Full waveform Lidar data and hyperspectral images, respectively. Full waveform LiDAR data and hyperspectral images both were collected at 1500 m above ground level on September 2 and 13, 2012. Both data were acquired in the morning, in which, the hyperspectral data recorded was from 7:36 to 10:38 a.m. (GMT+8). The spatial resolution of hyperspectral image is 1 meter and spectral range of hyperspectral data is 362.8 to 1051.3 nm. As this data belong to Narrow-band, which bandwidth is 9.6 nm, the total of 72 bands. In addition, LiDAR intensity sampling frequency is 1 GHz. Field of view was set 40 degree. So, we can obtain the point density of 2 pts/m^2.

Fusion process is divided into two parts (Figure 2). First, hyperspectral image and full waveform data was performed by data pre-processing. a) We eliminated 902.8 to 979.4 nm because these bands in the hyperspectral imagery may be influenced by water vapor. b) We calculated the intensity of LiDAR in the extent of 1 m × 1 m, and translated the intensity raster image.

The second phase of process, denpendency between each band of data was raised by multivariate statistical analysis. We used Minimum Noise Component (MNF) transformation (Green et al., 1988) for data rotation. It is preferred over Principal Components Analysis (PCA). PCA primarily employ the principle component linear conversion model to carry each band of orthogonal transformation out, and to cover maximum of information in front of several bands, that can improve data quality and decrease the data dimension. Different from PCA, the signal images was tranformed. The image covariance matrix is regarded as the sum of signal and noise contributions. The signal image was separated by MNF transformation, as this transformation model can be used to maximize the signal to noise ratio (Canty, 2006). However, the intensity image canot be administered when band value is zero after band 120, because $\sum_S$ and Σ_N must be symmetric and positive definite. According to the above conditions, MNF was used for hyperspectral images, and PCA was used for the intensity image. Equations are

following below:

$$Y = A + G \quad (1)$$

$$\sum = \sum_S + \sum_N \quad (2)$$

where Y is new image after rotation, A is principal components transformation matrix, G is original image, Σ is covariance matrix for original image, Σ_S is covariance matrix for singal image, and Σ_N is covariance matrix for noise image.

The factor loading can explain weight of each component, so we can acquire the eigen value of each component band that is band contribution. High contribution of component bands were be selected after accomplish transformation models, and the fusion image was stacked by these useful bands. We compared classification of fusion image and hyperspectral image to show that the fusion image was helpful via accuracy analysis. Image classification method employed unsupervised classification (maximum likelihood method). The accuracy analysis included user's Accuracy, producer's Accuracy, Overall Accuracy, and Kappa.

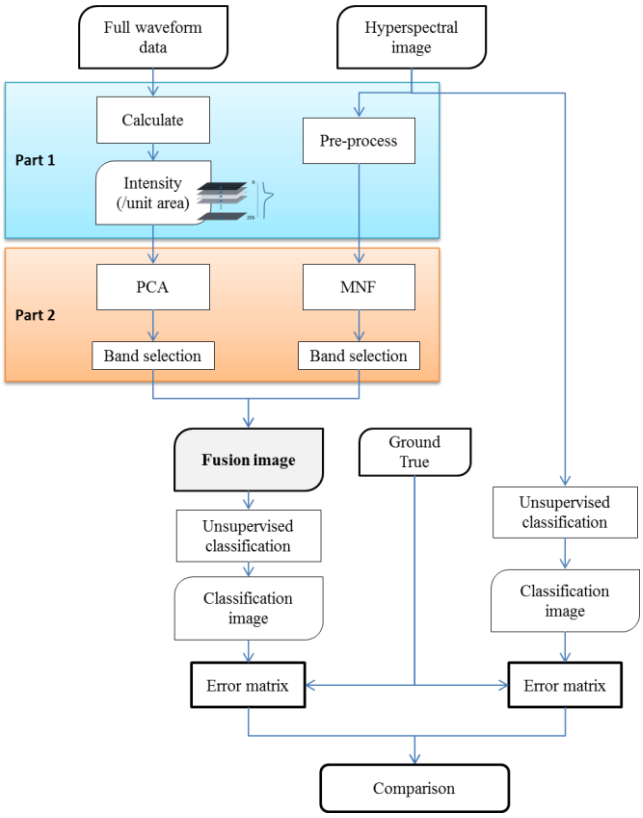

Figure 2. This study was included two process, 1) data pre-processing, 2) multivariate statistical analysis for images. Finally, we were via the accuracy analysis to compare the result.

RESULTS AND DISCUSSION

Table 1 shows the contribution of each band and selected bands. Contribution of hyperspectral image and LiDAR intensity image were respective 95.65% and 96.09%. Hyperspectral image and lidar intensity image was completed spectral band of component conversion respectively. Strip boundary is conspicuous (figure 3), so filtering each component axes is necessary. Avoidance lost well axes even though it was low contribution, we also filtered each component axes to choose excess bands. We can see that first component axes of each transformation model has high contribution ratio, those had 70% contribution for after rotation images each.

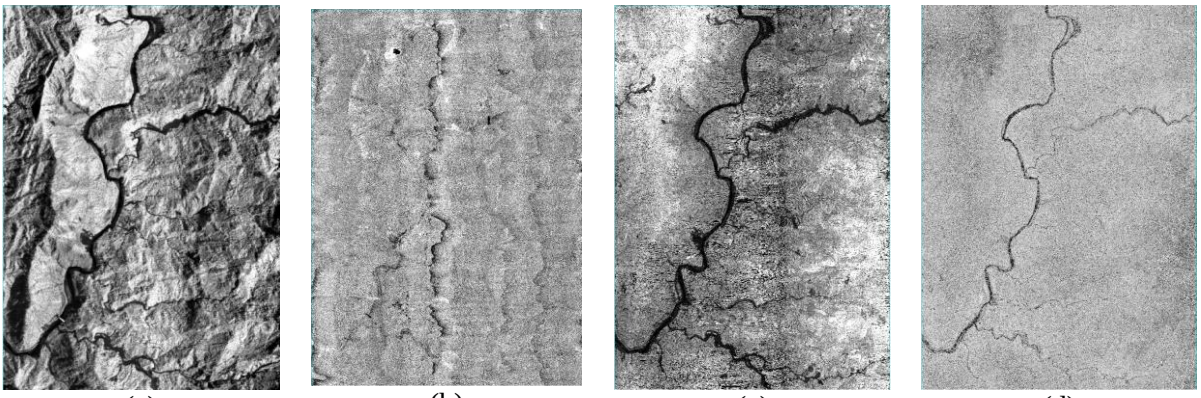

(a) (b) (c) (d)

Figure 3. Sample of Good and bad bands after transformation, (a) Good for hyperspectral band, (b) Bad for hyperspectral band, (c) Good for LiDAR intensity band, (d) Bad for LiDAR intensity band.

Table 1. Contribution of each component axes.

Component axes	Hyperspectral image（MNF）		LiDAR intensity image（PCA）	
	Contribution (%)	Cumulative Contribution (%)	Contribution (%)	Cumulative Contribution (%)
1	**73.784**	**73.78**	**70.225**	**70.22**
2	**10.768**	**84.55**	**11.216**	**81.44**
3	**5.417**	**89.97**	**8.548**	**89.99**
4	**2.533**	**92.5**	**4.22**	**94.21**
5	**1.469**	**93.97**	**1.849**	**96.06**
6	**1.08**	**95.05**	1.206	97.26
7	0.73	95.78	0.809	98.07
8	0.652	96.43	0.495	98.57
9	**0.383**	**96.82**	0.382	98.95
10	0.361	97.18	0.247	99.2
11	0.287	97.46	0.198	99.4
12	**0.22**	**97.68**	0.136	99.53
13	0.173	97.86	0.101	99.63
14	0.145	98	0.067	99.7
15	0.14	98.14	0.057	99.75
16	0.118	98.26	0.036	99.79
17	0.095	98.36	0.025	99.81
18	0.088	98.44	0.023	99.84
19	0.085	98.53	**0.019**	**99.86**
20			0.016	99.87
21			**0.014**	**99.89**
22			0.011	99.9
23			0.009	99.9
24			0.008	99.92
25			0.006	99.92
⋮	⋮	⋮		
63	0.01	100.00	⋮	⋮
⋮				
255			0	100
Total Contribution		95.65		96.09

Figure 4 shows that classification of fused image and hyperspectral image results. The maximum likelihood method of supervised image classification processing was compared the results of the fused

image and hyperspectral image, because fused image quality can be determined by land cover classification. In this figure 4 shows that fused image improved classified accuracy of WR, and the shallow river and BS of both sides of river can be clearly divided. Furthermore, TF and AF, also ameliorated successfully classification of TF and AF in forest areas. Not only some small TF can classified by classification of fusion image, AF areas are also intact classified better than hyperspectral images. In addition, we randomly generated 420 check points to estimate classification accuracy.

Table 2 is comparatively result for confusion matrix. Kappa of fusion image and hyperspectral image are separately 0.9 and 0.8. Overall accuracy of fusion image and hyperspectral image are 89.1% and 80%. Moreover, high user's accuracy explain low misclassification, and high producer's accuracy interpret low omission classification ratio. user's accuracy and producer's accuracy of fusion image is universal high. So, that shows commission and omission of fusion image is better than hyperspectral image.

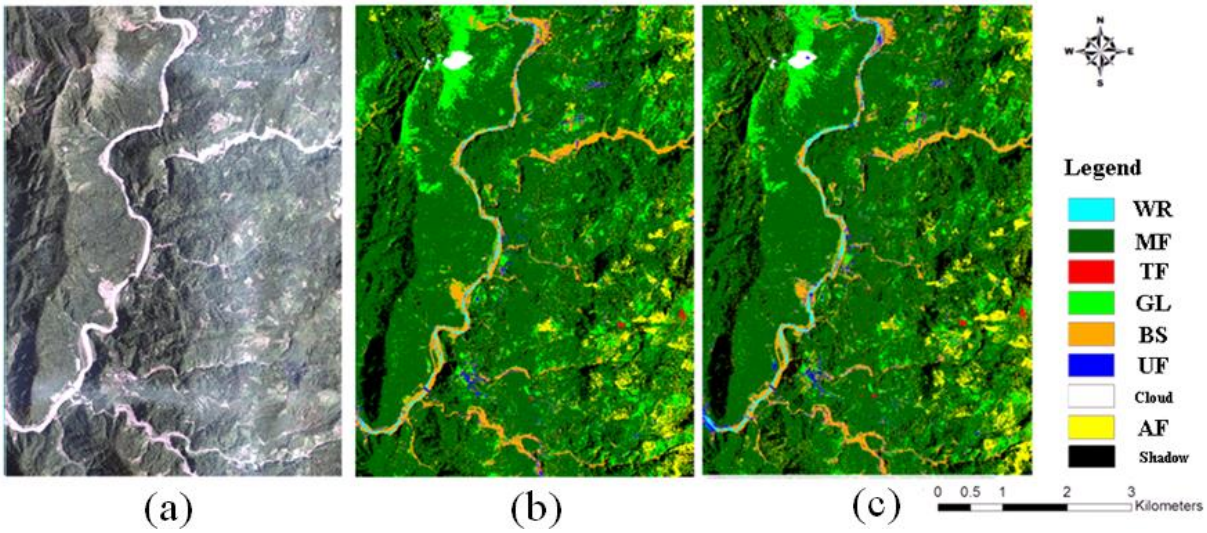

Figure 4. (a) Ortho image and results of classification images: (b) hyperspectral and (c) fused image.

Table 2. Classification accuracy

	User's accuracy (%)			Producer's accuracy (%)		
	Fusion	Hyper.	Δ	Fusion	Hyper.	Δ
WR	98.1	97.5	0.61	86.7	65.0	21.7
MF	76.3	60.4	15.9	96.7	96.8	0
TF	98.1	97.7	0.41	85.0	70.0	15
GL	98.1	96.4	1.75	90.0	90.0	0
BS	73.3	63.3	10	91.7	95.0	-3.3
UF	92.3	91.7	0.64	80.0	73.3	6.7
AF	98.3	97.9	0.38	93.4	76.7	16.7

	Overall Accuracy	Kappa
Hyper.	81%	0.8
Fusion	89.1%	0.9
Δ	8.1%	0.1

Table 3 and Table 4 are the confusion matrix for classification image of fused and hyperspectral. Fused classified correct ratio has 80% to 96.8% for each land cover type, and hyperspectral classified correct ratio has 65% to 96.8%. MF and GL can classified successly which 96.8% and 90% in the two classified results. Classified result of WR was mistaken for BS. UF and BS, TF and MF have still wrong classification. But, it is worth to be mentioned that wrong ratio of fused image is low.

Although the classification of BS and UF has still need to be breakthrough, on the whole, fusion of hyperspectral images and full waveform LIDAR data is helpfully for land use classification.

Table 3. Confusion matrix for classification of fused image.

Classes \ Ground truth	WR	MF	TF	GL	BS	UF	AF
WR	**87%**	0	0	0	1.6%	0	0
MF	0	**96.8%**	15%	8%	0	0	7%
TF	0	1.6%	**85%**	0	0	0	0
GL	0	1.6%	0	**90%**	0	0	0
BS	12%	0	0	0	**91.7%**	20%	0
UF	0	0	0	0	6.7%	**80%**	0
AF	1%	0	0	2%	0	0	**93%**

Table 4. Confusion matrix for classification of hyperspectral image.

Classes \ Ground truth	WR	MF	TF	GL	BS	UF	AF
WR	**65%**	0	0	0	1.6%	0	0
MF	0	**96.8%**	30%	8%	1.6%	0	23%
TF	0	0	**70%**	2%	0	0	0
GL	0	3.2%	0	**90%**	0	0	0
BS	28%	0	0	0	**95.2%**	27%	0
UF	5%	0	0	0	1.6%	**73%**	0
AF	2%	0	0	0	0	0	**77%**

CONCLUSION

Full waveform LiDAR data can effectively obtain high-precision 3D terrain, through full waveform LIDAR data can improvement in land cover classification which easily misclassified regions. Assessment of the results by the image fusion has successfully proved that the classification is better than the hyperspectral image classification results. Appropriate image conversion can reduce the spectral dimension and to keep data characteristics. Therefore, combination and developmental of two different data fusion imaging techniques is necessary.

REFERENCES

[1] Borengasser, M., Hungate, W.S., Watkins, R., 2008, Hyperspectral Remote Sensing Principles and Applications. CRC Press, Boca Raton, Florida, USA.

[2] Giovanni Forzieri, Gabriele Moser, Filippo Catani, Assessment of hyperspectral MIVIS sensor capability for heterogeneous landscape classification, *ISPRS Journal of Photogrammetry and Remote Sensing*, 74 (2012) 175‑184.

[3] J. REITBERGER, P. KRZYSTEK, and U. STILLA, 2008 , Analysis of full waveform LIDAR data for the classification of deciduous and coniferous trees, *International Journal of Remote Sensing*, 29(5) 1407–1431.

[4] Joshua R.Ben-Arie, GeoffreyJ.Hay, RyanP.Powers, GuillermoCastilla, Benoıˆt St-Onge, 2009, Development of a pit filling algorithm for LiDAR canopy height models, *Computers & Geosciences*, 35 (2009) 1940–1949.

[5] Morton J. Canty, 2006, Image Analysis, Classification and Change Detection in Remote Sensing: With Algorithms for ENVI/IDL, CRC Press.

[6] Pohl, C., and Genderen, J.L.V., 1998, Multisensor image fusion in remote sensing: concepts, methods and applications, *International Journal of Remote Sensing*, 19(5) 32.

[7] Udayalakshmi Vepakomma, Benoit St-Onge, Daniel Kneeshaw, 2008, Spatially explicit characterization of boreal forest gap dynamics using multi-temporal lidar data, *Remote Sensing of Environment*, 112 (2008) 2326-2340.